A spontaneous mutation in MutL-Homolog 3 (HvMLH3) affects synapsis and crossover resolution in the barley desynaptic mutant *des10*

1. Isabelle Colas[1],
2. Malcolm Macaulay[1],
3. James D. Higgins[2],
4. Dylan Phillips[3],
5. Abdellah Barakate[4],
6. Markus Posch[5],
7. Susan J. Armstrong[6],
8. F. Chris H. Franklin[6],
9. Claire Halpin[4],
10. Robbie Waugh[1,4,*] and
11. Luke Ramsay[1,*]

Author Information

1 Cell and Molecular Sciences, The James Hutton Institute, Invergowrie, Dundee, UK

2 University of Leicester, Leicester, UK

3 Institute of Biological, Environmental and Rural Sciences (IBERS), Aberystwyth University, Aberystwyth, UK

4 Division of Plant Sciences, University of Dundee at The James Hutton Institute, Dundee, UK

5 Light Microscopy Facility, College of Life Sciences, Dundee, UK

6 School of Biosciences, University of Birmingham, Edgbaston, Birmingham, UK

[*] Authors for correspondence:
Luke Ramsay
Tel: +44 844 928 5428
Email: Luke.Ramsay@hutton.ac.uk (mailto:Luke.Ramsay@hutton.ac.uk)

Robbie Waugh
Tel: +44 844 928 5428
Email: Robbie.Waugh@hutton.ac.uk (mailto:Robbie.Waugh@hutton.ac.uk)

Keywords: barley (*Hordeum vulgare*); crossover; meiosis; MutL-Homolog 3 (MLH3); recombination; super resolution microscopy.

Summary

- Although meiosis is evolutionarily conserved, many of the underlying mechanisms show species-specific differences. These are poorly understood in large genome plant species such as barley (Hordeum vulgare) where meiotic recombination is very heavily skewed to the ends of chromosomes.
- The characterization of mutant lines can help elucidate how recombination is controlled. We used a combination of genetic segregation analysis, cytogenetics, immunocytology and 3D imaging to genetically map and characterize the barley meiotic mutant DESYNAPTIC 10 (*des10*).
- We identified a spontaneous exonic deletion in the orthologue of MutL-Homolog 3 (HvMlh3) as the causal lesion. Compared with wild-type, *des10* mutants exhibit reduced recombination and fewer chiasmata, resulting in the loss of obligate crossovers and leading to chromosome mis-segregation. Using 3D structured illumination microscopy (3D-SIM), we observed that normal synapsis progression was also disrupted in *des10*, a phenotype that was not evident with standard confocal microscopy and that has not been reported with Mlh3 knockout mutants in Arabidopsis.
- Our data provide new insights on the interplay between synapsis and recombination in barley and highlight the need for detailed studies of meiosis in nonmodel species. This study also confirms the importance of early stages of prophase I for the control of recombination in large genome cereals.

Introduction

Meiotic recombination is one of the principal forces underlying genetic diversity and a driver for evolution as well as progress in crop breeding programmes (Riley et al., 1981). A deeper understanding of this process offers the opportunity to manipulate recombination and improve the speed and accuracy of plant breeding in order to address the needs of food security within a period of increased environmental constraints (Able et al., 2009; Martinez-Perez, 2009). This is particularly true in cereals such as wheat, barley, oats and rye, as well as in many forage grasses that show a highly skewed distribution of meiotic crossovers (COs) relative to gene content, with large portions of the chromosomes around the centromeric regions rarely recombining (Kunzel et al., 2000; Kunzel & Waugh, 2002; Higgins et al., 2012; IBGSC et al., 2012; Ramsay et al., 2014). Interestingly this CO distribution phenotype is not found in Arabidopsis nor in either rice or *Brachypodium*, grass species with much smaller genomes (Chen et al., 2002; Huo et al., 2011; Salomé et al., 2012). The control of recombination and the interlinked processes of early meiotic progression have been intensively studied in model eukaryotic organisms with comparative studies being undertaken in mammalian species and the standard model plants Arabidopsis and rice (Gerton & Hawley, 2005; Baudat et al., 2013; Luo et al., 2014; Mercier et al., 2014), but they have yet to be deciphered in large genome cereals.

During meiosis, homologous recombination starts with the formation of programmed DNA double-stranded breaks (DSB) by the protein SPO11 that is found in all eukaryotes (Metzler-Guillemain & de Massy, 2000; Stacey et al., 2006; Keeney, 2008). The DSB ends are resected by the MRE11 complex (MRE11-Rad50-Xrs2 in yeast, MRE11-Rad50-NSB1 in plants) to generate 3′ ssDNA tails (Daoudal-Cotterell et al., 2002; Raynard et al., 2008; Nicolette et al., 2010) which are then coated by the recombinases RAD51 and DMC1 to mediate strand invasion resulting in a joint molecule (D-Loop) (Shinohara

et al., 1997; Kathiresan et al., 2002; Da Ines et al., 2012). The subsequent repair occurs either by synthesis-dependent strand annealing (SDSA) resulting in noncrossovers (NCO) or via a double Holliday junction (dHj) (Hunter, 2007; Bzymek et al., 2010; Matos & West, 2014). Protein complexes (MSH4-MSH5, MER3) stabilize the dHjs (Nakagawa & Kolodner, 2002; Snowden et al., 2004) that are mostly resolved into COs by the MutL homologs MLH1–MLH3 (Ranjha et al., 2014; Rogacheva et al., 2014), with a certain fraction resolved into NCO by a helicase-dependent mechanism in Arabidopsis (Knoll & Puchta, 2011). Orthologues for many of these proteins have been identified in plants, suggesting a broadly conserved mechanism for crossover formation (Higgins et al., 2014; Luo et al., 2014; Mercier et al., 2014). It has been postulated that in Arabidopsis 85% of crossovers arise from a pathway under the control of the ZMM (ZYP, MSH, MER) group of proteins (Higgins et al., 2004, 2005; Mercier et al., 2005). This pathway produces Class I COs which exhibit interference, the phenomenon where the presence of a CO reduces the probability of an additional CO in an adjacent interval with the remaining COs being Class II that do not exhibit interference (Higgins et al., 2008).

Homologous pairing, recombination and synapsis have been studied extensively, but the interdependence between these processes remains to be fully resolved and may differ between species (Santos, 1999; Zickler, 2006). In cereals, telomeres cluster during early meiosis to bring homologous chromosomes together and initiate synapsis (Colas et al., 2008; Higgins et al., 2012). During zygotene the two homologues progressively synapse along their entire length and the process is completed at pachytene (Santos, 1999; Zickler, 2006). The synaptonemal complex then disassembles but the chromosomes remain held together by chiasmata (the cytogenetic manifestation of the COs). At metaphase I the bivalents align at the equatorial plate and each of the homologous chromosomes then separates at anaphase I. A second round of cell division then follows, resulting in sister chromatid separation and the formation of haploid cells (Stack & Anderson, 2001).

Although much of our current understanding has been developed in small genome models, it is now being extended to large and complex genome nonmodel crops such as barley, where recent cytogenetic studies have described meiotic progression and the chronology of meiotic events (Higgins et al., 2012; Phillips et al., 2012; Barakate et al., 2014). Although largely conforming to expectations, specific observations such as the clustering of the telomeres and the spatiotemporal organization of the recombination machinery reveal that barley differs from Arabidopsis(Armstrong et al., 2001; Higgins et al., 2012; Phillips et al., 2012; Barakate et al., 2014). Even in related grasses (e.g. barley vs rice) there are conflicting reports of the direction of change in the number of chiasmata formed after disrupting the amount of the synaptonemal complex protein ZIPPER1 (HvZYP1/OsZEP1) (Wang et al., 2010; Barakate et al., 2014) hinting at significant functional differences between related components of the overall meiotic machinery.

In order to explore meiosis in a large genome crop we have been using a collection of barley DESYNAPTIC mutants that were determined cytologically in the 1970s to have an aberrant meiotic phenotype with the presence of univalents being ascribed to premature desynapsis (Lundqvist et al., 1997). Here we have taken a classical forward-genetics approach to map the spontaneous semi-sterile DESYNAPTIC 10 (*des10*) mutant (Lundqvist et al., 1997) and identify the causal mutation as a deleted exon in the mismatch repair gene HvMlh3. Using a combination of genetic segregation analysis and super-resolution immunocytology, we show that the mutation has a deleterious effect on recombination and crossing over. The unique form of the *des10* mutant allele results in the coding sequence being maintained in frame, allowing immunofluorescent visualization of the protein in both mutant and wild-type, providing novel insights into its importance in the very early stages of meiosis.

Materials and Methods

Plant material

Plants (Hordeum vulgare L.) were grown under 16 h of light at 18–20°C and 8 h of dark at 16°C. For cytology, the cv Bowman (wild-type (WT)) and its near-isogenic line BW230 (*des10*) were grown in a growth cabinet until meiosis. Anthers were checked for meiosis stage and fixed in formaldehyde. To assess the effect of *des10* on recombination, F_2 and F_3 populations derived from BW230× cv Morex were grown in a glasshouse and young leaf tissue were collected in 96 well plates for DNA extraction and genotypic analysis. Plants were grown to maturity to assess fertility.

Mapping and sequencing

Frozen plant material was disrupted in a lysis buffer using a Qiagen grinder and DNA extracted with Qiagen DNA extraction kit using an automated station QIAxtractor® (Qiagen). Initial genetic mapping utilized a custom 384 single nucleotide polymorphism (SNP) genotyping array using the Illumina beadXpress platform. For mapping we used the segregation of the semi-sterile phenotype of *des10* as a Mendelian trait. Using JOINMAP 4.0 (Kyazma BV, Wageningen, Netherlands) software, loci were assigned to linkage groups and two rounds of regression mapping were used to order the loci within groups. The iterative development of custom KASPar© SNP assays (LGC, Middlesex, UK) derived from alignments of genic sequences, known to map in this interval, were mined for polymorphism between cv Bowman and Morex, and these used to delineate the interval containing *des10* to a single 1.02 Mb BAC contig (contig_38558) containing six annotated genes (http://mips.helmholtz-muenchen.de/plant/barley/fpc/index.jsp (http://mips.helmholtz-muenchen.de/plant/barley/fpc/index.jsp)). Primers were designed to amplify the genomic sequences of the six genes within the BAC contig and all other possible syntenic genes and the PCR products sequenced using the big dye v.3.1 reaction kit and analysed on an ABI Prism 3730 (Applied Biosystems, Foster City, CA, USA). For cDNA sequencing, mRNA from young inflorescences and anthers from BW230 (*des10*) and Bowman was extracted using an RNA extraction kit (Qiagen) in the presence of DNAseI. cDNA was made using the standard protocol of the Superscript III kit (Life Technologies, Thermo Fisher Scientific, Waltham, MA, USA) and sequenced using specific primers encompassing the deleted region.

Recombination frequency

F_3 individuals derived from selfed seed from F_2 individuals homozygous for *des10* or WT alleles at HvMlh3 were used for the recombination assay. The genome-wide genetic mapping utilized the custom 384 SNP genotyping array. Three independent c. 20-cM intervals on 4H (centromeric), short arm of 6H (distal) and long arm of 7H (distal) were studied in more depth using KASP© assays.

Immunocytology

Anthers were fixed in 4% formaldehyde (1×phosphate-buffered saline (PBS) /0.5% Triton™ X-100) for 20–30 min, rinsed twice in 1×PBS/0.5% Triton™ X-100 and tapped to release the meiocytes. Meiocytes suspension (30 µl) were transferred onto a Polysine® slide (poly-$_{L}$-lysine coated slides) and left to air dry (room temperature) and without squashing to preserve the 3D conformation. Slides were first blocked for 30 min in 3% bovine serum albumin in 1×PBS, 0.1% Triton™ X-100 and then incubated in the primary antibody solution which consisted of one or multiple antibodies (raised in rabbit or rat) diluted in blocking solution in a wet chamber for 1 h at room temperature followed by 24–48 h at 4°C. The antibodies that have been previously described were; anti-AtASY1, -AtZYP1, -HvMLH3, -AtRAD51, -AtMHS4 and -AtDMC1 (Higgins et al., 2012; Phillips et al., 2012, 2013; Barakate et al., 2014). We also prepared a new barley antibody, anti-HvZYP1 (Rat), from an immunization with two individual peptides (Dundee Cell Products, Dundee, UK) to confirm the ZYP1 phenotype. Slides were warmed for 30 min to 1 h at room temperature before washing for 15 min in 1× PBS and incubating for up to 2 h at room temperature in a secondary antibody solution consisting of a mixture of anti-rabbit Alexa Fluor® (488 or 568) and/or anti-rat Alexa Fluor® (568 or 488) (Invitrogen) diluted in 1×PBS. Slides were washed for 15 min in 1×PBS, counterstained with Hoechst 33342 (Life Technologies) for 15 min, and mounted in Vectashield® (H-1000; Vectorlabs, Burlingame, CA, USA).

DNA in situ hybridization

For chiasmata counts, anthers were fixed in ethanol : acetic acid (3 : 1) for 24 h and stored in 70% ethanol at 4°C until use. Slide preparation and DNA in situ hybridizations were performed as previously described (Higgins et al., 2012) using rDNA 5s-digoxigenin and rDNA 45s-biotin probes to identify the individual chromosomes.

Time course

Stems were injected with 0.5–1 ml of 10 µM 5-ethynyl-2′-deoxyuridine (EdU) in the region of the inflorescence (under the base of the spike) and also two-thirds of the way up along the length of the stem. The EdU solution was left in the stems for 2 h to allow for its incorporation into S-phase nuclei as described previously (Higgins et al., 2012). Spikes were collected and fixed in fresh 4% formaldehyde/PBS fixative for 30 min to 1 h at various time-points (6, 18, 24, 48 and 68 h after the 2 h of EdU pulse). Fixed anthers were prepared for immunodetection with anti-ASY1 (primary and secondary incubation) as described earlier, immediately followed by EdU detection as per the suppliers protocol. EdU was detected with Click-iT® EdU Alexa Fluor® 488 HCS assay kit (Life Technologies) with 45 min incubation instead of 30 min in the supplied protocol. Slides were counterstained with Hoechst 33342 (2 µg ml^{-1}, Life Technologies), mounted in Vectashield® (H-1000, Vectolabs) and sealed.

Microscopy

For confocal microscopy, 3D Confocal stack images (512 × 512, 12-bit) were acquired on a LSM-Zeiss 710 fitted C-Apochromat ×63/1.20 W Korr M27 oil objective. Laser light (405, 488, 561 and or 594 nm) was used at 2–4%, sequentially with two (up to four) lines averages. 3D stack slices were taken at 0.25–0.44 µm intervals at a pixel dwell of 1.58 µs. For synaptonemal complex (SC) spreads, imaging was performed using a Nikon Eclipse 90i microscope as described previously (Higgins et al., 2012; Barakate et al., 2014). For structured illumination microscopy, 3D structured illumination microscopy (3D-SIM) images were acquired on a DeltaVision OMX Blaze (GE Healthcare,Buckinghamshire, UK) fitted with an Olympus PlanApo N ×60 1.42 NA oil objective. Laser light from solid state lasers (405, 488 and 564 nm), shuttered by high-speed tilt mirrors and coupled into a broadband single mode optical fibre, was split into three beams. 3D interference patterns in the sample plane were generated by focusing of the beams onto the back focal plane of the objective lens. Striped illumination patterns were shifted by five phase steps and rotated by three angles (−60°, 0° and +60°), providing a set of 15 images per unprocessed z-section. Interference patterns were phase-shifted by directing the outer two beams through a separate pair of windows with individual tilt control. Phase of Survey the interference pattern at the sample plane was shifted due to the change in the path length for the respective outer beam, whereas lateral refractive beam translation was cancelled by tilting a given window pair in complementary directions. Angles of pattern orientation were shifted by a tilt mirror, directing the three beam patterns to one of three mirror clusters; the beam pattern from each of the three rotation paths was redirected back to a common exit path by reflecting a second time from the tilt mirror. Exposure times were typically between 100 and 200 ms, and the power of each laser was adjusted to achieve optimal intensities of between 1000 and 3000 counts in a raw image of 15-bit dynamic range of Edge sCMOS camera (PCO AG, Germany). The lowest possible laser power was chosen for each channel to minimize photo bleaching. Unprocessed image stacks were composed of 15 images per z-section (five phase-shifted images for each of three interference pattern angles). The microscope was routinely calibrated by measuring channel specific optical transfer functions (OTFs) to optimize lateral and axial image resolution (channel dependent and typicallyc. 120 and 300 nm, respectively). Super-resolution 3D image stacks were reconstructed with $_{SOFTWORX}$ 6.0 (GE Healthcare) using channel specific OTFs and Wiener filter setting of 0.002 (0.005 for the 4′,6-diamidino-2-phenylindole channel) to generate a super-resolution 3D image stack. Images from the different colour channels, recorded on separate cameras, were registered with the $_{SOFTWO}R_X$ 6.0 alignment tool (GE), based on alignment parameters obtained from calibration

Imaging and modelling

Images were processed with the respective microscope software package, or with external imaging tools like Fiji ($_{IMAGEJ}$ 1.49 m, (https://imagej.nih.gov/ij/) for deconvolution (Vonesch & Unser, 2008; Schindelin et al., 2012) and $_{IMARIS}$ 8.1.2 (Bitplane) for 3D projection and MLH3 counting. Barley MLH3 protein modelling was obtained by submitting the protein sequence of the intact protein and the truncated version to the SWISS-MODEL workspace (Bordoli et al., 2009).

Results

des10 is the result of a mutation in the mismatch repair gene HvMlh3

des10 is a spontaneous semi-sterile mutant of the barley cv Betzes (Lundqvist et al., 1997). The original mutation was backcrossed repeatedly to cv Bowman then selfed to produce the Bc_5F_3 near-isogenic line BW230 (*des10*) (Fig. 1a) (Druka et al., 2011). To identify the lesion causing the observed phenotype, we genetically mapped the *des10* mutation using an F_2 population (n = 168) derived from a cross between BW230 (*des10*) and the cv Morex to the long arm of chromosome 5H (Fig. 1b) using a standard SNP marker set (Close et al., 2009; Druka et al., 2011). By extending the population to 1102 F_2 plants and using additional KASP™ SNP markers developed using published genome sequence data from cv Morex and Bowman (IBGSC et al., 2012), we located *des10* to a 0.2-cM interval encompassed entirely within a 1.02 Mb BAC contig (contig_38558) containing six annotated genes (Fig. 1b). Sequencing all six genes revealed a single polymorphism between BW230 (*des10*) and Betzes in MLOC_52425 (Fig. 1b) consisting of a 159-bp deletion that removes the entire seventeenth exon of a putative gene model encoding HvMutL-homolog 3 (HvMLH3 – GenBank accession no. JQ855501 (http://www.ncbi.nlm.nih.gov/entrez/query.fcgi?cmd=search&db=Nucleotide&dopt=GenBank&term=JQ855501), Supporting Information Fig. S1a), but maintaining the open reading frame of the downstream exons (Figs S1b, 2a). The deleted exon encodes the majority of the conserved $DQHAX_2EX_4E$ metal binding motif essential for the endonuclease activity of HvMLH3 (Fig. 2b), a mismatch repair protein that has a role in the resolution of double Holliday junctions (dHj) arising from the ZMM dependent CO pathway (Lipkin et al., 2000; Jackson et al., 2006; Nishant et al., 2008; Phillips et al., 2013). Deletion of this domain is predicted to affect protein conformation (Fig. 2c,d), potentially destabilizing the MutLγ protein complex (MLH1-MLH3) required for resolution of dHjs (Guarne et al., 2004; Ranjha et al., 2014).

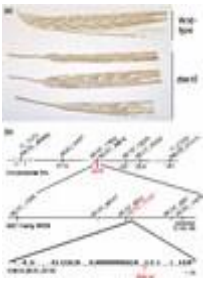

Figure 1. *des10* mapping. The barley (Hordeum vulgare) mutant *des10* exhibits a semi-sterile phenotype (a) producing fewer seeds per ear (7.0 ± 2.7) in *des10* than wild-type (13.7 ± 3.7). The *des10* (in red) region was initially delineated (b) between two single nucleotide polymorphism (SNP) markers (11_11273 and 11_21203) on the long arm of chromosome 5H and then fine mapped on an extended F_2 population to a 0.2 cM region between two markers (MLOC_17896 and MLOC_34818) located on the same BAC contig (contig_38588). The only exonic polymorphism for the genes within this BAC contig was a deletion in MLOC_52425 (in red) encoding the barley orthologue of HvMLH3.

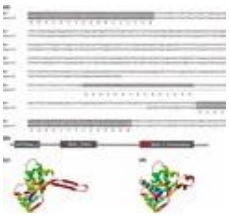

Figure 2. *des10* mutation. (a) Alignment of the barley (Hordeum vulgare) HvMlh3 gene sequences in wild-type (WT) and *des10*, with exons highlighted in grey. The 159-bp deletion removes the entire 17th exon coding for the peptide sequence HAADERIRLEELRSK without affecting reading frame. (b) The histidine kinase-like ATPases and the MutL_Trans domains are unaffected but the *des10* Mutl-C domain is missing the majority of the metal binding motif QHAADERIRLEE (red box). This 15 amino acid deletion potentially affects the Mutl-C conformation in (c) *des10* as compared with (d) WT (default Swissmodel colouring).

des10 has fewer chiasmata than observed in WT

In order to confirm and further characterize the meiotic phenotype of *des10* mutants we used fluorescence in situ hybridization (FISH) with probes against 45S and 5S rDNA to determine chiasma frequencies and CO at metaphase I in WT and *des10*. Although homologues are normally paired at pachytene in both genotypes (Fig. 3a,e), *des10* exhibits fewer chiasmata. In the WT metaphase I, the number of chiasmata ranged from 16 to 20 per nucleus with the mean frequency of 18.4 ± 1.3 (n = 21) (Fig. 3b,i,j) slightly lower than CO numbers (mean = 21.8) estimated from genetic maps (Close et al., 2009; IBGSC et al., 2012) but closer than previous estimates (Nilsson et al., 1993). In *des10* we observed significantly fewer chiasmata ranging from 5 to 13 per nucleus with a mean of 9.2 ± 2.1 (n = 57) (Fig. 3f,i,j) and we also observed the presence of univalents (1.7 ± 2.0, n = 57) (Fig. 3f,i) leading to occasional aberrant chromosome segregation at anaphase I (Fig. 3c,g), genetically unbalanced tetrads (Fig. 3d,h) and a subsequent semi-fertile phenotype. Given the similar size of the seven chromosome pairs, the distribution of chiasmata per nucleus in*des10* can be compared with that expected assuming a Poisson distribution of the number of chiasmata observed (Jones, 1967). The observed distribution was significantly different from that expected from a random distribution (P = 0.034), which indicated that although the presence of univalents is indicative of a substantial disruption, some control of CO distribution remained (Jones, 1967; Jackson et al., 2006).

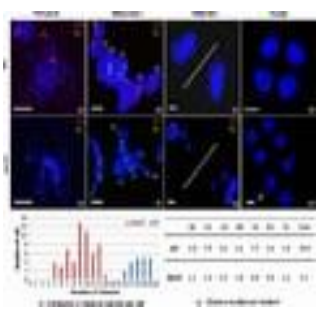

Figure 3. Reduced chiasmata and abnormal chromosome segregation in *des10*. 3D confocal optical section of (a–d) barley (Hordeum *vulgare*) wild-type (WT) and (e–h) the barley mutant *des10* meiocytes (bars, 10 μm). At pachytene, homologous chromosomes are paired in both (a) WT and (e) *des10* as shown with the 45 s (red) and 5 s (green) probes. (b) WT metaphase I has seven ring bivalents that can be identified with 45S (red) and 5S (green) probes, whereas (f). *des10* metaphase I averages 9.2 chiasmata per nucleus with occasional univalents. During anaphase I, chromosomes segregate to each pole in (c) WT, whereas chromosome mis- segregation is evident in (g) *des10*. Tetrads are normal and genetically balanced in (d) WT but not in (h) *des10* (white arrow indicating unbalanced complement). (i) Histogram of the distribution of chiasmata per cell for *des10* and WT and (j) a table of the number of chiasmata per chromosome in WT and *des10*.

des10 shows reduced genetic recombination frequency

Given the recessive nature of the mutation, we investigated the effect of *des10* on genetic recombination using segregating F_3 families derived from specific F_2 individuals from the BW230 (*des10*) × Morex cross that were homozygous for either the WT (n = 188 across 15 F_2 familes) or *des10* mutant (n = 183 across 16 F_2 familes) allele at HvMlh3. The reconstituted chromosome linkage maps generated from the segregation data within the F_3 families derived from WT F_2 individuals were comparable to the barley consensus map (Close et al., 2009; IBGSC et al., 2012). However, the maps derived from the segregation data within the F_3 families derived from *des10* F_2 individuals showed considerably less recombination, being only 45.9% of the length of the maps derived from WT families (excluding chromosome 5H due to the selection at the HvMlh3 locus) (Figs 4, S2). There was little evidence to suggest that the reduction in recombination varied across the genome with similar reductions observed in subtelomeric (44.2%) or centromere-proximal regions (51.4%) (Fig. S2) with the estimates of genetic to physical distance ratios in WT and *des10* changing from 1.16 to 0.46 cM Mb^{-1} in distal subtelomeric regions and from 0.06 to 0.03 cM Mb^{-1} in proximal regions. The reduction in recombination frequency was confirmed by comparisons at three specific intervals delineated by KASPar© SNP markers on a larger number of individuals from F_3 families (WT, n = 695 across 22 F_2 families; *des10*, n = 556 across 24 F_2 families) that all showed significant differences in recombination with *des10* lines, showed a mean reduction to 39% WT recombination frequency (26.0–54.6% ($P = 8.4^{e-8}$–0.01)) (Fig. S3). The reduction in recombination in these F_3 families paralleled the reduction of chiasmata observed cytogenetically in the mutant *des10* compared with WT.

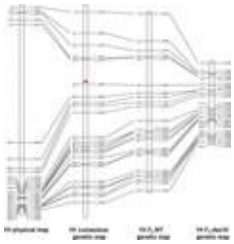

Figure 4. Genetic mapping in F_3 families. Alignment of the physical sequence (in Mbp) with consensus genetic map (in cM) for barley (Hordeum vulgare) chromosome 1H with comparisons to the genetic maps calculated from BW230 (*des10*) × Morex F_3 families derived from F_2 individuals homozygous for either the wild-type (WT) or *des10* mutant allele at HvMlh3. Estimated centromere position on genetic map marked in red.

Chromosome pairing is normal but the normal progression of synapsis appears compromised in *des10*

Given the importance of the interplay between synapsis and recombination in CO formation (Santos, 1999; Zickler, 2006), we compared synapsis in *des10* and WT using antibodies raised against AtZYP1 and the axial element associated protein AtASY1 (Higgins et al., 2012; Phillips et al., 2012; Barakate et al., 2014) using structured illumination microscopy (SIM). Axis formation and the initiation of synapsis during leptotene were comparable in WT (Figs 5a,b, S4) and *des10* (Figs 5g,h, S4). By mid-zygotene in WT most of the chromosomes were paired (Fig. 5c,d) and the typical tri-partite structure of the SC was visible (Fig. 5d, white arrow) with the ZYP1 signal suggesting new synapsis initiation sites, as shown previously (Phillips et al., 2012). The tri-partite structure was also clearly visible at pachytene in WT with complete synapsis evident (Fig. 5e,f). Using confocal microscopy, synapsis appeared to progress normally with the linearization of the ZYP1 signal during zygotene–pachytene (Fig. S5). However, with SIM there appeared to be a difference in the relative positioning of ZYP1 compared with WT with a highly punctate ZYP1 signal observed in *des10* at mid-zygotene (Fig. 5i,j) or later (Fig. 5k,l) that precluded the discernment of the SC tri-partite structure at mid-zygotene (Fig. 5j) or late zygotene/pachytene (Fig. 5l). The problems of homologue pairing were also indicated by unsynapsed ASY1 regions resembling the previously described 'peg and coalescent' process (Colas et al., 2008) at early zygotene in *des10* (Fig. 5j, arrows). However, the punctuated appearance of ZYP1 seen with SIM was not obvious when using confocal images, where the ZYP1 signal appeared linear in *des10* (Fig. S5). This suggests that the homologous chromosomes are aligned but that either the SC is not fully mature in the mutant or that in *des10* the chromatin structure is altered precluding binding of the ZYP1 antibody. Using Imaris we were able to track the individual bivalents of the later zygotene/pachytene cells in *des10* (Fig. 5k) and show that the distance between the ASY1 labelled homologues was maintained at 0.1 μm (Fig. 6), as previously reported at pachytene (Phillips et al., 2012), suggesting that despite the nonlinear ZYP1, these cells are fully synapsed.

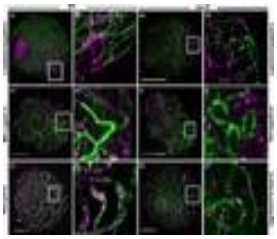

Figure 5. Comparison of synapsis in wild-type (WT) and *des10*. Progression of synapsis in WT and *des10* demonstrated by the immunolocalization of AtASY1 (green) and AtZYP1 (magenta) on formaldehyde fixed barley (Hordeum vulgare) meiocytes. Cells visualized by 3D structured illumination microscopy (3D-SIM) show the progression of synapsis in (a–f) WT and (g–l) *des10* at (a, b, g, h) leptotene, (c, d, i, j) zygotene and (e, f, k, l) pachytene together with detailed views of white squared regions (squares in a, c, e, g, i, k) shown in (b, d, f, h, j, l). Bars, 5 μm.

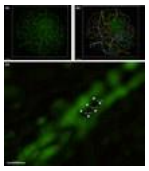

Figure 6. Imaris modelling of *des10* pachytene like cell. (a) 3D view from Imaris of *des10* cell from Fig. 5(k) with ASY1 labelling. (b) Individual barley (Hordeum vulgare) bivalent labelling in different colours using Imaris tracking. (c) The distance between the two homologous chromosomes is 0.1 μm corresponding to the WT synaptonemal complex distance. Bars: (a, b) 3 μm; (c) 0.4 μm.

des10 displays delayed synapsis

The observations of a perturbed synaptic progression were unexpected given that synapsis has been reported as normal in both Arabidopsis and mouse knockout mlh3 mutants (Lipkin et al., 2002; Jackson et al., 2006), albeit that the former was analysed using confocal microscopy only. In order to better understand how and when the mutation in *des10* was having this effect, we conducted a time-course analysis using EdU labelling. After collecting spikes of the same size in both WT and *des10* for each time point, meiocytes were spread from the central spikelets (numbers 3–10). This enabled several stages of meiosis to be studied for each spike with the EdU intensity/distribution and ASY1 linearity/intensity under confocal microscopy being used to classify the cells. A total of 27, 163, 98 and 141 cells were counted in WT and 26, 172, 167 and 46 cells in *des10*, at 18, 24, 48 and 68 h, respectively. We observed that early meiotic events in *des10* were comparable to WT with the presence of the telomere bouquet, which produces a concentrated ASY1 signal at one side of the nucleus (Higgins et al., 2012), at 6 h (Fig. 7a–c) and 18 h (Fig. 7d–f). However, although by 48 h (Fig. 7j–l) in WT there were roughly equal numbers of cells in zygotene and pachytene with 8% in later stages, in *des10*, 87% of the total cells were in zygotene with no cells found at

pachytene, although 5% were at later stages. This result corresponds to the apparent defect in synapsis described earlier, suggesting that in chromosome condensation). At 68 h (Fig. 7m–o), similar levels of metaphase I were found in WT and *des10*, cells appear suspended at zygotene with very few exhibiting a mature pachytene (with a strong linear ZYP1 signal relating to, but although 100% of them are labelled in WT, 29% of the total metaphase I cells were not labelled in *des10*, indicating that in *des10* they have lost synchronicity, potentially due to the delay in synapsis. Although this lack of synchronicity made estimates difficult for the majority of the cells, the total length of prophase does not appear generally different between WT and *des10*. Thus, unlike the 25-h delay in reaching metaphase I in knockout AtMlh3 mutants (Jackson et al., 2006), *des10* cells exhibit no overall (or little) time delay compared with WT. Moreover, a comparison of the stages of meiotic progression relative to changes in meiocyte size based on DNA staining (Fig. S6) revealed that the expected chromosomal changes were delayed in *des10* relative to WT (Kleckner et al., 2004; Jackson et al., 2006; Higgins et al., 2012).

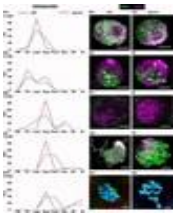

Figure 7. 5-ethynyl-2′-deoxyuridine time course in wild-type (WT) and *des10*. Percentage of barley (Hordeum vulgare) cells in each meiotic stage category and 3D confocal optical sections of WT and *des10* meiocytes at (a–c) 6 h, (d, f) 18 h, (g–i) 24 h, (j–l) 48 h and (m–o) 68 h. Bars, 5 μm. PM, pre-meiotic; TB, telomere bouquet; Lept, leptotene; Zyg, zygotene; Pach, pachytene; Dip, diplotene; MI, metaphase I; AI, anaphase I. The solid vertical black line indicates the zygotene stage in all panels.

HvMLH3 foci detectable in WT and *des10*

Using high-resolution immunocytology, we observed that the HvMLH3 antibody (Phillips et al., 2013) produced a punctate signal associated with the nucleus at zygotene in WT barley with some MLH3 signal associated with chromatin and the forming SC (Fig. 8a–d). At late zygotene/early pachytene, synapsis of the chromosomes in WT progressed via ZYP1 polymerization and although the MLH3 signals are detectable in the nucleus, a subset of more distinct MLH3 foci become evident on the SC (Fig. 8e–h, triangles). At late pachytene, (Fig. 8i–l), polymerization of ZYP1 is complete and distinct MLH3 foci are evident as described previously (Phillips et al., 2013). Using 3D stacks, the final MLH3 foci count (Figs 8j triangles, S7) averaged 20.8 (± 3.4, n = 19) per cell (Table S1) for the WT, which corresponds closely to the average chiasma count of 18.4 at metaphase I.

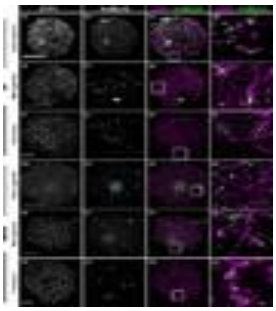

Figure 8. Distribution of ZYP1 and HvMLH3 during prophase. (a–l) Wild-type (WT) and (m–x) *des10* barley (Hordeum vulgare) meiotic progression monitored using antibodies raised against HvZYP1 (magenta) and HvMLH3 (green) using 3D structured illumination microscopy (3D-SIM) with detailed views of white squared regions (squares in c, g, k, o, s, w shown in d, h, l, p, t, x). At early zygotene in both (a–d) WT and (m–p) *des10* MLH3 signal is abundant (b, n) in the nucleus including associations with the chromosomes axes (d, p). This continues into early pachytene, in both (e–h) WT and (q–t) *des10*. However, in the WT (g, h) a few foci with a stronger signal potentially marking the finalized crossovers (COs) become evident (triangles) whereas it is difficult to differentiate foci in *des10* (s, t). At late pachytene (i–l, u–x), CO foci (triangles) are seen clearly in WT as compared with weaker unassociated signals (circle) (k, l). Weaker synaptonemal complex associated foci (w–x) are discernible in *des10* (triangles) though considerable MLH3 signal remains in the nucleus and on the axes. Bars, 5 μm.

The exonic deletion in Stage *des10* almost entirely removes the functional HvMLH3 metal binding motif, but as the mutation leaves *HvMlh3* in frame, it potentially produces detectable protein that is endonuclease deficient and under the control *des10* static of its native promoter. This was confirmed with immunocytology with the HvMLH3 antibody in conjunction with HvZYP1 allowing the observation of the mutant protein in relation to the synaptonemal complex formation. As the problems of synapsis in *des10* that are evident when using 3D-SIM could complicate accurate staging when using the ZYP1 antibody without ASY1, the staging was also carried out using confocal images where the ZYP1 signal appears linear in *des10* (Fig. S5).

At zygotene, we observed a similar MLH3 signal in the nucleus in *des10* (Fig. 8m–p) as in the WT (Fig. 8a–d). However, at late zygotene/pachytene, judged by the stage of ZYP1 polymerization, distinct foci were much less apparent in *des10* (Fig. 8q–t) with a higher background MLH3 signal present in the nucleus (Fig. 8t). At the pachytene-like stage in *des10*, distinct foci did form and the final number could be estimated using 3D image stacks (Figs 8v triangles, S8) with the mean being 7.7 foci per cell (± 1.6, n = 30) (Table S1) which is close to the observed average of 9.2 chiasmata per nucleus. The distribution of the number of MLH3 foci per nucleus in *des10* was significantly different from a Poisson distribution (P = 0.011), confirming our earlier conclusion from chiasmata counts that the COs are not random (Jackson et al., 2006). Interestingly although the number of cells was limited and the count subject to experimental error, the MLH3 foci distribution in *des10* did, however, just fit a binomial distribution expected given the number of foci found in the mutant and WT.

In addition, we found that DSB formation was not disturbed in *des10* and progressively formed in both WT and *des10* from the distal regions and localized to the axial elements as previously described in barley (Figs S9, S10) (Higgins et al., 2012; Phillips et al., 2012; Barakate et al., 2014). However, higher numbers of RAD51, DMC1 and MSH4 foci were found in *des10*, compared with WT, (Table 1; Figs S9, S10) suggesting that the mutation is either affecting DSB numbers, as previously reported in ZMM mutants (Thacker et al., 2014), or the dynamics of DSB repair.

Table 1. Recombination foci in wild-type (WT) and *des10* barley; table showing the mean number (with ± SD) of AtDMC1, AtRAD51 and AtMSH4 foci in WT and *des10* at the telomere bouquet, the stage of declustering of the telomere and the linear ASY1 stage

Stage	Protein	WT	des10	TTEST static
Telomere bouquet	RAD51	127.27 ± 55.38	142.2 ± 49.3	2.46E-01
Declustering	RAD51	164.96 ± 63.12	240.8 ± 80.6	6.48E-04
Linear ASY1	RAD51	349.3 ± 79.5	700.3 ± 128.2	1.721E-05
	DMC1	361.3 ± 62.9	766.8 ± 147.3	4.4873E-06
	MSH4	323.2 ± 33.4	639.5 ± 79.5	3.53682E-06

Discussion

des10 is a spontaneous mutation in HvMlh3

Using classical forward-genetics, we show that the spontaneous semi-sterile barley *des10* mutant is the consequence of a deletion of exon 17 of MutL-homolog 3 (HvMlh3) that contains most of the conserved C-terminal metal binding endonuclease domain. The *des10* mutant showed a clear meiotic phenotype with a reduction in chiasmata number relative to the wild-type (WT) that mirrors the reduction seen in the knockout mutants in Arabidopsis, the only other plant for which mlh3 mutants have been characterized (Jackson et al., 2006). As in Arabidopsis, the presence of some univalents indicates that the remaining crossovers (COs) are insufficient in number in some cells to ensure accurate chromosome segregation.

This similar level of reduction in chiasmata in the MLH3 mutants indicates that, as expected, the deletion of the majority of the conserved metal binding motif essential for the endonuclease activity (Nishant et al., 2008) in *des10* mimics the complete knockout of the gene. The effects observed were, however, less severe than those found in classical ZMM mutants in Arabidopsis and Zyp1 knockdowns in barley (Higgins et al., 2004; Barakate et al., 2014) which also corresponds with the phenotypes observed in Arabidopsis MLH1 and MLH3 mutants (Jackson et al., 2006; Dion et al., 2007). Importantly, given the nature of the mutation, we were able to count the MLH3 foci directly in both WT and in *des10* unlike in the Arabidopsis and mouse knockout studies. These MLH3 foci counts confirmed the reduction observed with chiasmata counts, showing a reduction to 37% (7.7/20.8) compared with WT that mirrored the estimates of chiasmata counts (50%: 9.2/18.4) and interestingly that were close to the ratio found with chiasmata counts in Arabidopsis (39%) (Jackson et al., 2006).

This mutant phenotype in both species is consistent with a post-ZMM role for MLH3 in the resolution of predetermined CO sites (Jackson et al., 2006; Zakharyevich et al., 2010). This interpretation was supported in Arabidopsis by the fit of the mutant cell chiasmata frequencies to a binomial distribution that modelled the probability (P) of the independent resolution of double Holliday junction (dHj) as COs at each of a preselected set of (k) recombination intermediates. However, in Arabidopsis, the chiasmata frequencies also fitted a simpler discrete Poisson distribution about the mean, potentially indicative of the random nature of the remaining COs. Importantly this simpler random distribution was not supported in this study, with both the counts of chiasmata and MLH3 foci in *des10* being significantly different from the expected Poisson distributions whereas the MLH3 foci distribution in *des10* did only just fit a binomial distribution expected given the number of foci found in the mutant and WT.

The effect of *des10* was observed genetically on recombination frequency with the F_3 map length of families derived from F_2 individuals homozygous for the *des10* allele at HvMlh3 being 45.9% the map length of WT. Interestingly there was little evidence to suggest that the reduction in recombination varied across the genome despite the known temporal–spatial control of recombination in barley (Higgins et al., 2012). This observation corresponds well with the assumption that MLH3 is involved in the resolution of predefined CO intermediates derived from the ZMM pathway and thus *des10* should not affect the distribution of designated CO events but will affect the proportion of these that are resolved as CO, that is will affect recombination frequency but not recombination distribution.

Intriguingly a similar proportion of WT CO was observed in *des10* (37%) as in AtMLH3 knockouts (39%). Although the mechanism by which the dHJs are resolved in the absence of a functional MLH3 is unclear (Jackson et al., 2006), the involvement of other complexes such as MLH1-PMS2 have been suggested (Lipkin et al., 2002). Considering the interaction between the MLH1-MLH3 complex and MMS4-MUS81 in yeast (Wang & Kung, 2002; Fabre et al., 2003; de los Santos et al., 2003), and the known involvement of MUS81 in mammalian (Holloway et al., 2008) and plant CO resolution (Higgins et al., 2008), it is possible that the resolution of the Class I COs in MLH3 mutants is mediated via the Class II machinery while maintaining the ZMM CO designations and interference (Zakharyevich et al., 2010).

HvMLH3 foci evident at zygotene

The development of MLH3 foci with the developing synaptonemal complex (SC) at zygotene is earlier than the classical expectation, where SC associated foci are generally observed at pachytene on completion of synapsis (Lipkin et al.,2002). However, this early development of MLH3 foci during zygotene is supported by observations in mouse and Arabidopsis (Kolas et al., 2005; Jackson et al., 2006) and of other MutL homologues in other species (Baker et al., 1995; Storlazzi et al., 2010). The earlier association of MLH3 signal with the nucleus at zygotene before the appearance of clear foci was surprising but showed a punctate but regular organization of stretches of ZYP1 signal separated by MLH3 foci (Fig. 7d). This would suggest that our observations are unlike the association with heterochromatic repeats found in mouse (Baker et al., 1995) or with chromatin organization suggested during chromosome segregation in humans (Roesner et al., 2014). This would therefore indicate that MLH3 is recruited earlier to the newly formed axes potentially during synapsis, rather than on mature chromosomes axes, as suggested by animal studies reporting the presence of MLH3 at pachynema.
In *des10*, the mutation affects the dimerization domain of HvMLH3 that would potentially cause a change in the conformation of the C-terminal domain and, thus, possible difficulties in forming the heterodimer with MLH1 that is required for the resolution of dHJs (Guarne et al., 2004; Ranjha et al., 2014; Rogacheva et al., 2014). However, the capacity of the complex to bind to chromatin would likely be unaffected given the intact DNA binding domain, and

as HvMLH3 is still recruited to the axis, its DNA binding activity appears to remain effective. This would parallel the behaviour of the yeast mutant MLH3Δ7 that also lacks the endonuclease motif, but is normally recruited to the DNA (Roesner et al., 2013). Interestingly the MLH3Δ7 studies also showed a higher turnover of the protein in the mutant that could tally with the higher background and staining of the nucleolus in this study. The early meiotic effects seen in *des10* may therefore be a manifestation of the timing of the binding of MLH3 with the continued presence of the defective protein on the axis generating a phenotype not detected in a knockout (Lipkin et al., 2002; Jackson et al., 2006).

des10 displays altered synapsis progression

The barley *des10* phenotype revealed a perturbation in the progression of synapsis compared with the WT that became evident at zygotene. This unexpected effect on synapsis and the associated delay in meiotic progression is broadly similar to phenotypes observed for ZMM mutants (Novak et al., 2001; Higgins et al., 2004; Barakate et al., 2014) although not as severe. Assembled ZYP1 appears to be fairly linear under confocal microscopy and subsequent meiotic progression indicates that the chromosomes are sufficiently aligned to allow some crossover resolution. However, with structured illumination microscopy ZYP1 did show a less continous signal than WT and was associated with a longer zygotene/pachytene transition in *des10*. Although the observed differences in synapsis could have been exacerbated by an increased sensitivity of the mutant protein containing complexes to the cytological procedures, such effects would de facto imply a change in structure. The observed perturbation of synapsis was consistent with the timing of the appearance of MLH3 signal and potentially relates to the changed binding dynamics of the mutant protein. Similarly the delay at zygotene observed in *des10* cells would be concomitent with the observed changes in structure associated with ZYP1 signal and the difficulty in observing cells with a classic pachytene appearance given the apparent problems of synapsis. It is thus unclear whether full synapsis is achieved in this desynaptic mutant or how many cells achieve full synapsis although cells clearly do progress through to diplotene.

The interplay between recombination and synapsis is a standard feature of meiotic mutant studies and is inherent in the grouping of ZIP1 (ZYP1) and mismatch repair genes in the ZMM pathway (Osman et al., 2011; Mercier et al., 2014). However, the processes of recombination and synapsis are not inseparable, with DSB formation and CO imposition known to occur before synapsis in some species (Santos, 1999; Fung et al., 2004; Thacker et al., 2014). Although our data show that CO imposition is retained in *des10*, it also suggests that SC progression is dependent on accurate CO resolution. Synapsis would therefore appear to involve different stages; with chromosome engagement, alignment and initiation being ZMM dependent (Thacker et al., 2014) but progression and maturation also being dependent on subsequent CO resolution by MLH3. We noted that RAD51/DMC1 counts were higher in *des10* and attribute this to the concomitant change in the observed timing of meiotic progression rather than a direct effect on DSB formation, as seen in ZMM mutants (Thacker et al., 2014). The observed difference in timing of MLH3 action compared with
Arabidopsis could reflect the specific nature of the *des10* mutation combined with the advantages of visualizing in a large genome with high-resolution microscopy. Whether our observations reflect an earlier role for MLH3 in plants in general or specifically in barley, they are consistent with the known spatiotemporal difference between barley and Arabidopsis in early meiosis. In barley, the distal and interstitial chromosomal regions exhibit temporal differentiation in recombination initiation that corresponds to the relative timing of replication and the differentiation of the genome by chromatin modifications (Higgins et al., 2012; Baker et al., 2015). This temporal separation of events along the chromosomes is in contrast to Arabidopsis where the formation of chromosome axes is very rapid and recombination initiation appears essentially synchronous throughout the chromosomes (Higgins et al., 2012). This potentially relates to the smaller genome size and distribution of heterochromatin, as well as the differing meiotic chromosome dynamics in the model species (Armstrong et al., 2001). In summary, we have taken advantage of genetic and genomic resources in barley to identify an exonic deletion in the orthologue of MutL-Homolog 3 (Mlh3) as the causal lesion in a natural semi-sterile DESYNAPTIC 10 (*des10*) mutant.
des10 exhibits reduced recombination and fewer chiasmata than the WT, congruent with our expectations for the post-ZMM role of HvMLH3 in the resolution of predetermined CO sites. The reduction in chiasmata resulted in the loss of obligate crossing-over leading to chromosome mis-segregation and the semi-sterile phenotype. This study thus confirms the conserved role of MLH3 in barley previously assumed in earlier studies (Phillips et al., 2013) and the non-random nature of the CO distribution in the mutant as postulated but not demonstrated in Arabidopsis (Jackson et al., 2006). Importantly, in barley MLH3 foci are evident at zygotene, earlier than expected, although this has been observed in other systems (Kolas et al., 2005); using 3D structured illumination microscopy (3D-SIM) super-resolution microscopy we were able to observe that *des10* also exhibited aberrant synaptonemal complex progression at this stage, associated with a meiotic delay. We interpret this as meaning that the resolution of CO is initiated early in barley and that its disruption in *des10* compromises synapsis progression with the associated change in the dynamics of the mutant MLH3 protein. Thus, in barley both crossover imposition and crossover resolution occur before full synapsis, affirming the importance of the early stages of prophase I for the control of recombination. The integration of genetic and cytological approaches to dissect the mutant phenotype of Hvmlh3 establishes the tractability of studying meiosis in large genome cereals. The size of the genome facilitates cytological discrimination of the profound changes in chromosome structure during prophase I and is potentially associated with specific changes in timing of meiotic processes when compared with physically smaller model systems.

Acknowledgements

We would like to thank Sybille Mittmann, Amritpal Sandhu and Ruth Perry for technical help. The research leading to these results has received funding from the European Community's Seventh Framework Programme FP7/2007-2013 under grant agreement no. 222883 to R.W., S.J.A. and F.C.H.F. Use of the OMX microscope was supported by the Euro-BioImaging PCS and through the MRC Next Generation Optical Microscopy Award (ref: MR/K015869/1) to I.C.,
L.R., M.M. and R.W. were funded from the Scottish Government's Rural and Environment Science and Analytical Services Division Work Program 5.2. A.B. and C.H. were funded by the Biotechnology and Biological Science Research Council Grant BB/F020872/1. The authors declare no conflict of interest.

References

Able JA, Crismani W, Boden SA. 2009. Understanding meiosis and the implications for crop improvement. Functional Plant Biology 36: 575–588.
Armstrong SJ, Franklin FC, Jones GH. 2001. Nucleolus-associated telomere clustering and pairing precede meiotic chromosome synapsis in Arabidopsis thaliana. Journal of Cell Science 114: 4207–4217.

Baker K, Dhillon T, Colas I, Milne I, Milne L, Bayer M, Flavell AJ. 2015. Chromatin state analysis of the barley epigenome reveals a higher-order structure defined by H3K27me1 and H3K27me3 abundance. Plant Journal 84: 111–124.

Baker SM, Bronner CE, Zhang L, Plug AW, Robatzek M, Warren G, Elliott EA, Yu J, Ashley T, Arnheim N et al. 1995. Male mice defective in the DNA mismatch repair gene PMS2 exhibit abnormal chromosome synapsis in meiosis. Cell 82: 309–319.

Barakate A, Higgins JD, Vivera S, Stephens J, Perry RM, Ramsay L, Colas I, Oakey H, Waugh R, Franklin FC et al. 2014. The synaptonemal complex protein ZYP1 is required for imposition of meiotic crossovers in barley. Plant Cell 26: 729–740.

Baudat F, Imai Y, de Massy B. 2013. Meiotic recombination in mammals: localization and regulation. Nature Reviews Genetics 14: 794–806.

Bordoli L, Kiefer F, Arnold K, Benkert P, Battey J, Schwede T. 2009. Protein structure homology modeling using SWISS-MODEL workspace. Nature Protocols 4: 1–13.

Bzymek M, Thayer NH, Oh SD, Kleckner N, Hunter N. 2010. Double Holliday junctions are intermediates of DNA break repair. Nature 464: 937–941.

Chen MS, Presting G, Barbazuk WB, Goicoechea JL, Blackmon B, Fang FC, Kim H, Frisch D, Yu YS, Sun SH et al. 2002. An integrated physical and genetic map of the rice genome. Plant Cell 14: 537–545.

Close TJ, Bhat PR, Lonardi S, Wu YH, Rostoks N, Ramsay L, Druka A, Stein N, Svensson JT, Wanamaker S et al. 2009. Development and implementation of highthroughput SNP genotyping in barley. BMC Genomics 10: 582.

Colas I, Shaw P, Prieto P, Wanous M, Spielmeyer W, Mago R, Moore G. 2008. Effective chromosome pairing requires chromatin remodeling at the onset of meiosis. Proceedings of the National Academy of Sciences, USA 105: 6075–6080.

Da Ines O, Abe K, Goubely C, Gallego ME, White CI. 2012. Differing requirements for RAD51 and DMC1 in meiotic pairing of centromeres and chromosome arms in Arabidopsis thaliana. PLoS Genetics 8: 245–256.

Daoudal-Cotterell S, Gallego ME, White CI. 2002. The plant Rad50–Mre11 protein complex. FEBS Letters 516: 164-166.

Dion E, Li L, Jean M, Belzile F. 2007. An Arabidopsis MLH1 mutant exhibits reproductive defects and reveals a dual role for this gene in mitotic recombination. Plant Journal 51: 431–440.

Druka A, Franckowiak J, Lundqvist U, Bonar N, Alexander J, Houston K, Radovic S, Shahinnia F, Vendramin V, Morgante M et al. 2011. Genetic dissection of barley morphology and development. Plant Physiology 155: 617–627.

Fabre F, Chan A, Heyer WD, Gangloff S. 2003. Alternate pathways involving Sgs1/Top3, Mus81/Mms4, and Srs2 prevent formation of toxic recombination intermediates from single-stranded gaps created by DNA replication. Proceedings of the National Academy of Sciences, USA 100: 1462

Fung JC, Rockmill B, Odell M, Roeder GS. 2004. Imposition of crossover interference through the nonrandom distribution of synapsis initiation complexes. Cell 116: 795–802.

Gerton JL, Hawley RS. 2005. Homologous chromosome interactions in meiosis: diversity amidst conservation. Nature Reviews Genetics 6: 477–487.

Guarne A, Ramon-Maiques S, Wolff EM, Ghirlando R, Hu XJ, Miller JH, Yang W. 2004. Structure of the MutL C-terminal domain: a model of intact MutL and its roles in mismatch repair. EMBO Journal 23: 4134–4145.

Higgins JD, Armstrong SJ, Franklin FC, Jones GH. 2004. The Arabidopsis MutS homolog AtMSH4 functions at an early step in recombination: evidence for two classes of recombination in Arabidopsis. Genes & Development 18: 2557–2570.

Higgins JD, Buckling EF, Franklin FC, Jones GH. 2008. Expression and functional analysis of AtMUS81 in Arabidopsis meiosis reveals a role in the second pathway of crossing-over. Plant Journal 54: 152–162.

Higgins JD, Osman K, Jones GH, Franklin FC. 2014. Factors underlying restricted crossover localization in barley meiosis. Annual Review of Genetics 48: 29–47.

Higgins JD, Perry RM, Barakate A, Ramsay L, Waugh R, Halpin C, Armstrong SJ, Franklin FC. 2012. Spatiotemporal asymmetry of the meiotic program underlies the predominantly distal distribution of meiotic crossovers in barley. Plant Cell 24: 4096–4109.

Higgins JD, Sanchez-Moran E, Armstrong SJ, Jones GH, Franklin FC. 2005. The Arabidopsis synaptonemal complex protein ZYP1 is required for chromosome synapsis and normal fidelity of crossing over. Genes & Development 19: 2488–2500.

Holloway JK, Booth J, Edelmann W, McGowan CH, Cohen PE. 2008. MUS81 generates a subset of MLH1-MLH3-independent crossovers in mammalian meiosis. PLoS Genetics 4: e1000186.

Hunter N. 2007. Meiotic recombination. In: Aguilera A, Rothstein R, eds. Molecular genetics of recombination. Berlin, Heidelberg: Springer, 381–442.

Huo NX, Garvin DF, You FM, McMahon S, Luo MC, Gu YQ, Lazo GR, Vogel JP. 2011. Comparison of a high-density genetic linkage map to genome features in the model grass Brachypodium distachyon. Theoretical and Applied Genetics 123: 455–464.

IBGSC, Mayer KFX, Waugh R, Langridge P, Close TJ, Wise RP, Graner A, Matsumoto T, Sato K, Schulman A et al. 2012. A physical, genetic and functional sequence assembly of the barley genome. Nature 491: 711–716.

Jackson N, Sanchez-Moran E, Buckling E, Armstrong SJ, Jones GH, Franklin FCH. 2006. Reduced meiotic crossovers and delayed prophase I progression in AtMLH3-deficient Arabidopsis. EMBO Journal 25: 1315–1323.

Jones GH. 1967. The control of chiasmata distribution in rye. Chromosoma 22: 69–90.

Kathiresan A, Khush GS, Bennett J. 2002. Two rice DMC1 genes are differentially expressed during meiosis and during haploid and diploid mitosis. Sexual Plant Reproduction 14: 257–267.

Keeney S. 2008. Spo11 and the formation of DNA double-strand breaks in meiosis. Genome Dynamics and Stability 2: 81–123.

Kleckner N, Zickler D, Jones GH, Dekker J, Padmore R, Henle J, Hutchinson J. 2004. A mechanical basis for chromosome function. Proceedings of the National Academy of Sciences, USA 101: 12592–12597.

Knoll A, Puchta H. 2011. The role of DNA helicases and their interaction partners in genome stability and meiotic recombination in plants. Journal of Experimental Botany 62: 1565–1579.

Kolas NK, Svetlanov A, Lenzi ML, Macaluso FP, Lipkin SM, Liskay RM, Greally J, Edelmann W, Cohen PE. 2005. Localization of MMR proteins on meiotic chromosomes in mice indicates distinct functions during prophase I. Journal of Cell Biology 171: 447–458.

Kunzel G, Korzun L, Meister A. 2000. Cytologically integrated physical restriction fragment length polymorphism maps for the barley genome based on translocation breakpoints. Genetics 154: 397–412.

Kunzel G, Waugh R. 2002. Integration of microsatellite markers into the translocation-based physical RFLP map of barley chromosome 3H. Theoretical and Applied Genetics 105: 660–665.

Lipkin SM, Moens PB, Wang V, Lenzi M, Shanmugarajah D, Gilgeous A, Thomas J, Cheng J, Touchman JW, Green ED et al. 2002. Meiotic arrest and aneuploidy in MLH3-deficient mice. Nature Genetics 31: 385–390.

Lipkin SM, Wang V, Jacoby R, Banerjee-Basu S, Baxevanis AD, Lynch HT, Elliott RM, Collins FS. 2000. MLH3: a DNA mismatch repair gene associated with mammalian microsatellite instability. Nature Genetics 24: 27–35.

Luo Q, Li YF, Shen Y, Cheng ZK. 2014. Ten years of gene discovery for meiotic event control in rice. Journal of Genetics and Genomics 41: 125–137.

Martinez-Perez E. 2009. Meiosis in cereal crops: the grasses are back. Genome Dynamics 5: 26–42.

Matos J, West SC. 2014. Holliday junction resolution: regulation in space and time. DNA Repair 19: 176–181.

Mercier R, Jolivet S, Vezon D, Huppe E, Chelysheva L, Giovanni M, Nogue F, Doutriaux MP, Horlow C, Grelon M et al. 2005. Two meiotic crossover classes cohabit in Arabidopsis: one is dependent on MER3, whereas the other one is not. Current Biology 15: 692–701.

Mercier R, Mezard C, Jenczewski E, Macaisne N, Grelon M. 2014. The molecular biology of meiosis in plants. Annual Review of Plant Biology 66: 5.1–5.31.

Metzler-Guillemain C, de Massy B. 2000. Identification and characterization of an SPO11 homolog in the mouse. Chromosoma 109: 133–138.

Nakagawa T, Kolodner RD. 2002. The MER3 DNA helicase catalyzes the unwinding of Holliday junctions. Journal of Biological Chemistry 277: 28 019–28 024.

Nicolette ML, Lee K, Guo Z, Rani M, Chow JM, Lee SE, Paull TT. 2010. Mre11-Rad50-Xrs2 and Sae2 promote 5′ strand resection of DNA double-strand breaks. Nature Structural & Molecular Biology 17: 1478–1485.

Nilsson NO, Sall T, Bengtsson BO. 1993. Chiasma and recombination data in plants – are they compatible. Trends in Genetics 9: 344–348.

Nishant KT, Plys AJ, Alani E. 2008. A mutation in the putative MLH3 endonuclease domain confers a defect in both mismatch repair and meiosis in Saccharomyces cerevisiae. Genetics 179: 747–755.

Novak JE, Ross-Macdonald PB, Roeder GS. 2001. The budding yeast Msh4 protein functions in chromosome synapsis and the regulation of crossover distribution. Genetics 158: 1013–1025.

Osman K, Higgins JD, Sanchez-Moran E, Armstrong SJ, Franklin FC. 2011. Pathways to meiotic recombination in Arabidopsis thaliana. New Phytologist 190: 523–544.

Phillips D, Nibau C, Wnetrzak J, Jenkins G. 2012. High resolution analysis of meiotic chromosome structure and behaviour in barley (Hordeum vulgare L.). PLoS ONE 7: e39539.

Phillips D, Wnetrzak J, Nibau C, Barakate A, Ramsay L, Wright F, Higgins JD, Perry RM, Jenkins G. 2013. Quantitative high resolution mapping of HvMLH3 foci in barley pachytene nuclei reveals a strong distal bias and weak interference. Journal of Experimental Botany 64: 2139–2154.

Ramsay L, Colas I, Waugh R 2014. Modulation of meiotic recombination. In: Kumlehn J, Stein N, eds. Biotechnological approaches to barley improvement. Biotechnology in agriculture and forestry 69. Berlin, Heidelberg, Germany: Springer, 311–329.

Ranjha L, Anand R, Cejka P. 2014. The Saccharomyces cerevisiae Mlh1–Mlh3 heterodimer is an endonuclease that preferentially binds to Holliday junctions. Journal of Biological Chemistry 289: 5674–5686.

Raynard S, Niu H, Sung P. 2008. DNA double-strand break processing: the beginning of the end. Genes & Development 22: 2903–2907.

Riley R, Law CN, Chapman V. 1981. The control of recombination. Philosophical Transactions of the Royal Society B: Biological Sciences 292: 529–534.

Roesner LM, Mielke C, Fahnrich S, Merkhoffer Y, Dittmar KEJ, Drexler HG, Dirks WG. 2013. Stable expression of MutLγ in human cells reveals no specific response to mismatched DNA, but distinct recruitment to damage sites. Journal of Cellular Biochemistry 114: 2405–2414. Direct Link:

Roesner LM, Mielke C, Faehnrich S, Merkhoffer Y, Dittmar KE, Drexler HG, Dirks WG. 2014. Localization of MLH3 at the centrosomes. International Journal of Molecular Sciences 15: 13932–13937.

Rogacheva MV, Manhart CM, Chen C, Guarne A, Surtees J, Alani E. 2014. Mlh1–Mlh3, a meiotic crossover and DNA mismatch repair factor, is a Msh2–Msh3stimulated endonuclease. Journal of Biological Chemistry 289: 5664–5673.

Salomé PA, Bomblies K, Fitz J, Laitinen RAE, Warthmann N, Yant L, Weigel D. 2012. The recombination landscape in Arabidopsis thaliana F_2 populations. Heredity 108: 447–455.

Santos JL. 1999. The relationship between synapsis and recombination: two different views. Heredity 82: 1–6.

de los Santos T, Hunter N, Lee C, Larkin B, Loidl J, Hollingsworth NM. 2003. The Mus81/Mms4 endonuclease acts independently of double-holliday junction resolution to promote a distinct subset of crossovers during meiosis in budding yeast. Genetics 164: 81–94.

Schindelin J, Arganda-Carreras I, Frise E, Kaynig V, Longair M, Pietzsch T, Preibisch S, Rueden C, Saalfeld S, Schmid B et al. 2012. Fiji: an open-source platform for biological-image analysis. Nature Methods 9: 676–682.

Shinohara A, Gasior S, Ogawa T, Kleckner N, Bishop DK. 1997. Saccharomyces cerevisiae recA homologues RAD51 and DMC1 have both distinct and overlapping roles in meiotic recombination. Genes to Cells 2: 615–629.

Snowden T, Acharya S, Butz C, Berardini M, Fishel R. 2004. hMSH4–hMSH5 recognizes Holliday junctions and forms a meiosis-specific sliding clamp that embraces homologous chromosomes. Molecular Cell 15: 437–451.

Stacey NJ, Kuromori T, Azumi Y, Roberts G, Breuer C, Wada T, Maxwell A, Roberts K, Sugimoto-Shirasu K. 2006. Arabidopsis SPO11-2 functions with SPO11-1 in meiotic recombination. Plant Journal 48: 206–216.

Stack SM, Anderson LK. 2001. A model for chromosome structure during the mitotic and meiotic cell cycles. Chromosome Research 9: 175–198.

Storlazzi A, Gargano S, Ruprich-Robert G, Falque M, David M, Kleckner N, Zickler D. 2010. Recombination proteins mediate meiotic spatial chromosome organization and pairing. Cell 141: 94–106.

Thacker D, Mohibullah N, Zhu X, Keeney S. 2014. Homologue engagement controls meiotic DNA break number and distribution. Nature 510: 241–246.

Vonesch C, Unser M. 2008. A fast thresholded landweber algorithm for wavelet-regularized multidimensional deconvolution. IEEE Transactions Image Process. 17: 539–549.

Wang M, Wang K, Tang D, Wei C, Li M, Shen Y, Chi Z, Gu M, Cheng Z. 2010. The central element protein ZEP1 of the synaptonemal complex regulates the number of crossovers during meiosis in rice. Plant Cell 22: 417–430.

Wang TF, Kung WM. 2002. Supercomplex formation between Mlh1–Mlh3 and Sgs1-Top3 heterocomplexes in meiotic yeast cells. Biochemical and Biophysical Research Communications 296: 949–953.

Zakharyevich K, Ma Y, Tang S, Hwang PY, Boiteux S, Hunter N. 2010. Temporally and biochemically distinct activities of Exo1 during meiosis: double-strand break resection and resolution of double Holliday junctions. Molecular Cell 40: 1001–1015.

Zickler D. 2006. From early homologue recognition to synaptonemal complex formation. Chromosoma 115: 158–174.